New measurement of the fine structure in the $3\,^3P$ state of ^{4}He

P. B. Kramer* and F. M. Pipkin
Lyman Laboratory of Physics, Harvard University, Cambridge, Massachusetts 02138
(Received 27 March 1978)

The technique of level-crossing spectroscopy has been used to measure the fine-structure intervals in the $3\,^3P$ state of ^{4}He through the observation of the level crossings at 2277 and 3700 G. The magnetic fields at the crossing points were used in conjunction with calculated g values to obtain for the $3\,^3P_0$-$3\,^3P_2$ fine-structure interval the value 8772.552 ± 0.040 MHz (4.5 ppm). These same data yielded for the lifetime of the $3\,^3P$ state the value 97.6 ± 4.5 nsec and for the cross section for coherence-destroying collisions the value $(718 \pm 78)\pi a_0^2$.

I. INTRODUCTION

Measurements of the fine structure of two-electron atoms such as helium provide a test of quantum electrodynamics and the procedures used to calculate with precision atomic fine structure.[1-4] Here, a series of calculations first outlined by Schwartz[5] is used to calculate the helium fine structure. The Pauli reduction of the Breit interaction is used in first-order perturbation theory[5,6] to calculate the fine structure to order $\alpha^4 mc^2$. The inclusion of the first-order anomalous magnetic moment of the electron gives a term of order $\alpha^5 mc^2$. The Breit operators give in second-order perturbation theory[7-10] terms of order $\alpha^6 mc^2$ and $(m/M)\alpha^4 mc^2$. Another contribution of order $\alpha^6 mc^2$ arises from spin-dependent terms derived from a reduction of the covariant two-particle Bethe-Salpeter equation.[11,12] Nuclear-recoil corrections[13] give additional terms of order $(m/M)\alpha^4 mc^2$.

A major complication in the precision calculation of the helium fine structure comes from the necessity of having wave functions of sufficient accuracy to determine with the requisite precision the expectation value of the Breit operators and the second-order contributions due to the Breit operators.[5,6] The nonrelativistic three-body problem has not been solved analytically and numerical techniques must be used to determine approximate first-order wave functions. Here, the variational wave functions derived by Schiff *et al.*[6] are used to determine the $\alpha^4 mc^2$ term and the method of Dalgarno and Lewis,[14] which employs a variational solution of an inhomogeneous Schrödinger equation, is used to calculate the second-order contribution due to the Breit operators.[7-10]

The fine-structure intervals in helium are also attractive as a means for determining the fine-structure constant.[3,10,15,16] The $2\,^3P$ state of helium, unlike the $2\,^2P$ state of hydrogen, cannot decay to the atomic ground state; as a result the lifetime of the $2\,^3P$ state is longer (97.8 nsec as opposed to 1.6 nsec) and the natural width of the fine-structure transitions in helium is much smaller. Consequently, one should be able to measure the fine-structure interval in helium to a precision over 50 times greater than in hydrogen. Unlike in hydrogen, however, the determination of α from the helium fine structure requires tedious computer calculations involving wave functions with over 400 Hylleraas-like terms. These calculations should be independently tested to ensure their accuracy.

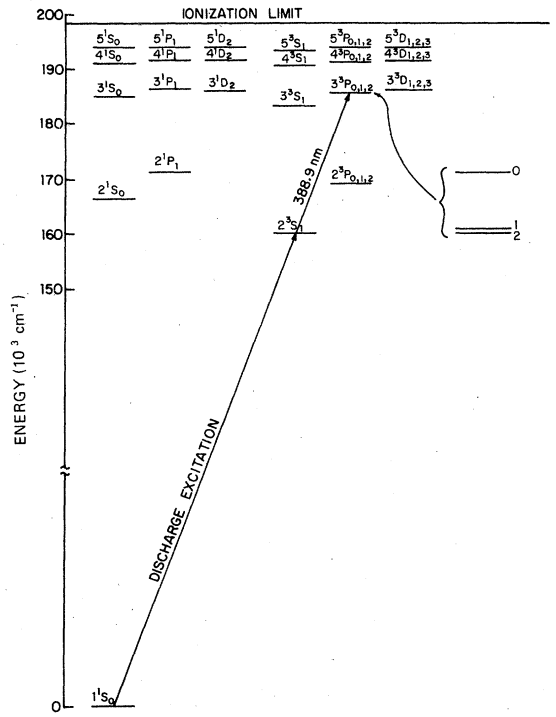

FIG. 1. Diagram showing the lower S, P, and D energy levels for helium. Also shown are the paths used to excite the $3\,^3P$ state for the measurements reported in this paper.

The measurement of the fine structure in the $n=3$ states provides an independent test of the calculations involved in determining α from the $n=2$ measurements.

This paper reports a new measurement of the fine structure in the $3\,^3P$ state of helium. Figure 1 shows a diagram of the energy levels of ^{4}He and the transition used to study the fine structure. Metastable helium atoms in the $2\,^3S_1$ state produced by a weak rf discharge were excited to the $3\,^3P$ state by 388.9-nm resonance radiation. The number of photons emitted at a fixed angle with respect to the incident light beam and an imposed magnetic field when the atoms decayed back to the $2\,^3S_1$ state was monitored as a function of the magnetic field. A change in the scattered light signaled the point at which two fine-structure levels crossed. The field values at which the levels crossed were used in conjunction with the Zeeman theory giving the dependence of the energy levels on magnetic field to determine the zero-field fine-structure intervals.

The successive sections of this paper describe in turn the theoretical framework, experimental apparatus, method of data analysis, systematic corrections, and conclusions.

II. THEORY

The level-crossing technique measures the value of the magnetic field that results in the degeneracy or crossing of two Zeeman sublevels. To determine the energy separation of the levels at zero magnetic field from the value of the field at which they cross, the Zeeman theory giving the dependence of the energy levels on the magnetic field must be used.

Lewis, Pichanick, and Hughes[17] have given a detailed description of the calculation of the Zeeman effect in the $2\,^3P$ state of helium and carried out these calculations to order $\alpha^2\mu_B H$ and $(m/M)\mu_B H$, where m is the electron mass, M is the mass of the helium nucleus, and μ_B is the Bohr magneton. Lewis *et al.*[17] also measured the g-factor and thus made an experimental test of their calculations. Lewis and Hughes[18,19] refined these calculations and partially extended them to other states in He. For our analysis of the $3\,^3P$ state, we made use of the notation and methods of these earlier articles.

The perturbation Hamiltonian resolving the degeneracy of the $3\,^3P$ state can be written in the form

$$\vec{\mathcal{H}} = \vec{\mathcal{H}}_{FS} + \vec{\mathcal{H}}_Z + \vec{\mathcal{H}}_Q \,. \tag{1}$$

Here $\vec{\mathcal{H}}_{FS}$ includes the spin-orbit and spin-spin terms and gives rise to the fine structure. $\vec{\mathcal{H}}_Z$ is the linear Zeeman term and can be written in the form

$$\vec{\mathcal{H}}_Z = g_L\mu_B\vec{L}\cdot\vec{H} + g_S\mu_B\vec{S}\cdot\vec{H} + \sum_{\gamma=1}^{6}\delta\vec{\mu}_\gamma\cdot\vec{H}\,, \tag{2}$$

where μ_B is the Bohr magneton and L and S are, respectively, the total orbital and spin angular momentum in units of $\hbar$. The first two terms in Eq. (2) are, respectively, the usual interaction of the orbital and spin magnetic moments with the external magnetic field H, which is assumed to be in the z direction. The orbital and spin g factors are assumed to have the values

$$g_L = (1 - m/M) = 0.999\,862\,9\,, \tag{3a}$$

$$g_S = 2[1 + \alpha/2\pi - 0.328(\alpha^2/\pi^2)\ldots] = 2.002\,319\,3\,. \tag{3b}$$

Equation (3a) includes most of the corrections for nuclear motion. There is a smaller more complicated motional correction which is included in the third term of Eq. (2). In Eq. (3b) α is the fine-structure constant $e^2/\hbar c$. The expression for g_S arises from the theoretical evaluation of the anomalous electron moment; the difference between this value and the most recent experimental value is negligible for our purposes.[20]

The first five of the $\delta\vec{\mu}_\gamma$ are the relativistic corrections given by

$$\delta\vec{\mu}_{1,2} = -\frac{1}{mc^2}\mu_B\sum_i\{(\vec{l}_i + 2\vec{s}_i)T_i - \tfrac{1}{2}Ze^2[\vec{s}_i\times\vec{\nabla}_i(r_i^{-1})]\times\vec{r}_i\} \tag{4a}$$

$$\delta\vec{\mu}_{3,4} = -\frac{e^2}{mc^2}\mu_B\sum_{i<j}\{(\vec{s}_i + 2\vec{s}_j)\times\vec{\nabla}_i(r_{ij}^{-1})\}\times\vec{r}_i\,, \tag{4b}$$

$$\delta\vec{\mu}_5 = -\frac{e^2}{\hbar mc^2}\mu_B\sum_{i<j}\{(r_{ij}^{-1}(\vec{r}_i\times\vec{p}_j) + r_{ij}^{-3})(\vec{r}_i\times\vec{r}_j)(\vec{r}_{ij}\cdot\vec{p}_j)\}\,, \tag{4c}$$

where $\vec{l}_i$, $\vec{s}_i$ are, respectively, the orbital and spin angular momentum operators for the ith electron, T_i is the kinetic-energy operator, and $\vec{r}_i$ ($\vec{r}_j$) is the spatial coordinate operator for the ith (jth) electron with $\vec{r}_{ij} = \vec{r}_j - \vec{r}_i$. Z is the atomic number. $\delta\vec{\mu}_6$ is the additional motional correction and is given by

$$\delta\vec{\mu}_6 = -\frac{m}{M}\mu_B\sum_{i<j}[(\vec{r}_i\times\vec{p}_j) + (\vec{r}_j\times\vec{p}_i)]\,. \tag{4d}$$

The quadratic term in Eq. (1) is

$$\vec{\mathcal{H}}_Q = \frac{e^2}{8mc^2}\sum_i(\vec{H}\times\vec{r}_i)\cdot(\vec{H}\times\vec{r}_i)\,. \tag{5}$$

To lowest order, the zero-field fine-structure Hamiltonian is diagonal in the basis $|LSJm_J\rangle$, where J is the total angular momentum. To calculate the energy levels as a function of magnetic field Lewis *et al.*[17] used a spherical-tensor-recoupling scheme to determine the matrix elements of the Hamiltonian in the $|LSJm_J\rangle$ representation. They obtained

$$\langle {}^3P_J m_J | \vec{\mathcal{H}}_Z | {}^3P_{J'} m_{J'} \rangle = (-)^{1-m_J}[(2J+1)(2J'+1)]^{1/2} \begin{pmatrix} J & 1 & J' \\ -m_J & 0 & m_{J'} \end{pmatrix}$$

$$\times \sqrt{6} \left(\begin{Bmatrix} J & I & J' \\ 1 & 1 & 1 \end{Bmatrix} [g'_S + (-)^{J+J'} g'_L] + (-)^J g_x \begin{Bmatrix} 1 & 1 & 2 \\ 1 & 1 & 1 \\ J & J' & 1 \end{Bmatrix} \right) \mu_B H , \tag{6a}$$

$$\langle {}^3P_J m_J | \vec{\mathcal{H}}_Q | {}^3P_{J'} m_{J'} \rangle = (-)^{J+J'-m_J}[(2J+1)(2J'+1)]^{1/2}$$

$$\times \frac{1}{2\sqrt{3}} \left[\begin{pmatrix} J & 0 & J' \\ -m_J & 0 & m_{J'} \end{pmatrix} \begin{Bmatrix} J & 0 & J' \\ 1 & 1 & 1 \end{Bmatrix} (R_{14} + R_{15}) + \left(\frac{2}{5}\right)^{1/2} \begin{pmatrix} J & 2 & J' \\ -m_J & 0 & m_{J'} \end{pmatrix} \begin{Bmatrix} J & 2 & J' \\ 1 & 1 & 1 \end{Bmatrix} R_{15} \right] \frac{(\mu_B H)^2}{R_\infty} , \tag{6b}$$

where

$$g'_L = g_L + \alpha^2(-R_2 - \tfrac{1}{3}R_5 + \tfrac{2}{15}R_7 - \tfrac{1}{3}R_8 + \tfrac{2}{15}R_9 + \tfrac{1}{30}R_{10} - \tfrac{1}{30}R_{11} - \tfrac{2}{15}R_{12} + \tfrac{2}{15}R_{13}) + (m/M)(\tfrac{1}{3}R_{16} - \tfrac{1}{3}R_{17} + \tfrac{2}{3}R_{18}) , \tag{7a}$$

$$g'_S = g_S + \alpha^2(-R_1 - R_2 + \tfrac{1}{3}R_3 + \tfrac{1}{3}R_4 - \tfrac{1}{2}R_5 - \tfrac{1}{2}R_6 + \tfrac{1}{3}R_7) , \tag{7b}$$

$$g_x = \alpha^2(R_4 - \tfrac{3}{2}R_6 - 2R_7 + \tfrac{3}{2}R_8) . \tag{7c}$$

R_∞ is the Rydberg for infinite mass and R_1–R_{18} are radial integrals. To determine the radial integrals we approximated the helium wave functions with hydrogenic wave functions. For the $3\,{}^3P$ state of He the antisymmetrized radial part of the wave function was taken to be

$$R(r_1, r_2) = \frac{1}{\sqrt{2}}[R_{1s}(r_1)R_{3p}(r_2) - R_{3p}(r_1)R_{1s}(r_2)], \tag{8}$$

where

$$R_{1s} = 2(Z_1)^{3/2} e^{-Z_1 r} , \tag{9a}$$

$$R_{3p} = (8/27\sqrt{6})(Z_3)^{5/2} r e^{-Z_3 r/3}(1 - Z_3 r/6) . \tag{9b}$$

Certain matrix elements have been accurately determined by Accad, Pekeris, and Schiff[21] as a by-product of their use of Hylleraas basis wave functions to calculate the energy of the $3\,{}^3P$ state. Their results have been taken as the correct values for $R_1 + R_2$ and $R_3 + R_4$; Z_1 and Z_3 have been adjusted so that the hydrogenic approximation gives these values. The resultant values for Z_1 and Z_3 were then used in the hydrogenic approximation to determine the radial integrals. Table I summarizes the values obtained with this method. The resulting hydrogenic prediction for $\langle r^2 \rangle$, which is equal to $\frac{1}{2}(R_{14} + R_{15})$, differs from the calculation of Accad, Pekeris and Schiff[21] by 3.5%. We have assigned an uncertainty of 1% to $R_1 + R_2$ and $R_3 + R_4$, 10% to R_{14} and R_{15}, and conservatively, 100% to R_5–R_{13} and R_{16}–R_{18}. In addition the separate determination of R_2 and R_4 were assigned an uncertainty of 50%.

The g values obtained for the $n = 3$ state using this method are

$$g'_S = g_S - (75.13 \pm 3.27) \times 10^{-6} = 2.002\,2442(33) , \tag{10a}$$

$$g'_L = g_L - (0.17 \pm 2.80) \times 10^{-6} = 0.999\,8627(28) , \tag{10b}$$

$$g_x = -(2.75 \pm 10.02) \times 10^{-6} = -0.000\,0028(100) . \tag{10c}$$

TABLE I. Summary of the matrix elements used for calculating the Zeeman effect. In this Table $|sp\rangle$ designates $R_{1s}(r_1)R_{3p}(r_2)$ and ∂r_2 designates $\partial/\partial r_2$. For the calculations, Z_1 and Z_3, respectively, were 1.9973 and 1.0684.

Matrix element	Numerical Value
$R_1 = \langle sp \vert \boldsymbol{T}_1 \vert sp \rangle$	1.9946
$R_2 = \langle ps \vert \boldsymbol{T}_1 \vert ps \rangle$	0.0634
$R_3 = \langle sp \vert 1/r_1 \vert sp \rangle$	1.9973
$R_4 = \langle ps \vert 1/r_1 \vert ps \rangle$	0.1187
$R_5 = \langle sp \vert 1/r_1 \vert sp \rangle$ $(r_2 \leq r_1)$	0.0014
$R_6 = \langle ps \vert 1/r_1 \vert ps \rangle$ $(r_2 \leq r_1)$	0.1169
$R_7 = \langle ps \vert r_1/r_2^2 \vert sp \rangle$ $(r_1 \leq r_2)$	0.0023
$R_8 = \langle sp \vert r_1^2/r_2^3 \vert sp \rangle$ $(r_1 \leq r_2)$	0.0065
$R_9 = \langle ps \vert r_1^3/r_2^4 \vert sp \rangle$ $(r_1 \leq r_2)$	0.0013
$R_{10} = \langle ps \vert r_2^2 \partial r_2/r_1^2 \vert sp \rangle$ $(r_2 \leq r_1)$	0.0008
$R_{11} = \langle sp \vert r_2^2 \partial r_2/r_1^2 \vert ps \rangle$ $(r_2 \leq r_1)$	−0.0051
$R_{12} = \langle ps \vert r_1^3 \partial r_2/r_2^3 \vert sp \rangle$ $(r_1 \leq r_2)$	0.0001
$R_{13} = \langle sp \vert r_1^3 \partial r_2/r_2^3 \vert ps \rangle$ $(r_1 \leq r_2)$	−0.0038
$R_{14} = \langle sp \vert r_1^2 \vert sp \rangle$	0.7520
$R_{15} = \langle ps \vert r_1^2 \vert ps \rangle$	157.6900
$R_{16} = \langle ps \vert r_1 \partial r_2 \vert sp \rangle$	0.0047
$R_{17} = \langle sp \vert r_1 \partial r_2 \vert ps \rangle$	−0.0366
$R_{18} = \langle ps \vert r_1/r_2 \vert sp \rangle$	0.0159

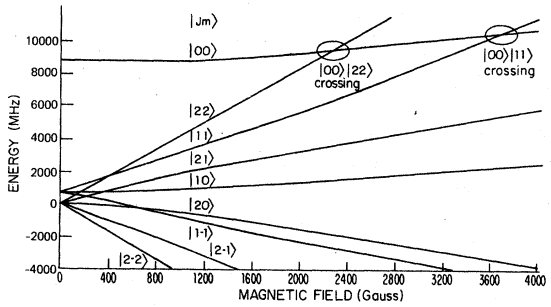

FIG. 2. Energy levels as a function of magnetic field for the $3\,^3P$ state of He. The labels for the state are exact only at zero magnetic field.

The accuracy of this calculation is difficult to assess. Coupling to other states, which would lead to a breakdown of the $1s3p$ configuration, has not been included. For the $n=2$ state this hydrogenic approximation has been compared to a calculation using Hylleraas wave functions; the two calculations give compatible values for the g factors. The value for $g_S' - g_S$ agrees with the value

$$g_S' - g_S = 75.08 \times 10^{-6} \tag{11}$$

obtained by Lewis and Hughes[19] from the expression

$$g_S' - g_S = -g_S \left[\alpha^2\left(\tfrac{1}{3}\langle T\rangle + \tfrac{1}{8}\langle 1/r_{12}\rangle\right) + (\alpha^3/4\pi)E\right], \tag{12}$$

derived using the virial theorem and evaluated using matrix elements calculated by Accad *et al.*[21] for T and r_{12}^{-1}.

Given the g factors it is straightforward to diagonalize the Hamiltonian and obtain the energy levels as a function of magnetic field. Figure 2 shows in graphic form the result of this calculation. In a magnetic field m_J is a good quantum number but J is not. In this paper we shall continue to use the $|J\,m_J\rangle$ quantum numbers to label the states at high field even though, in actual fact, the eigenstates are superpositions of the zero-field wave functions described by these quantum numbers. At roughly 2277 and 3700 G the $|00\rangle$ level crosses, respectively, the $|22\rangle$ level and the $|11\rangle$ level. It is these crossings that are used to determine the zero-field fine-structure intervals.

III. LEVEL-CROSSING SIGNAL

When two sublevels of an atomic state, which can both be reached from a single level through absorption of a photon and decay through emission of radiation to a single sublevel, cross, there will, in general, be an interference term in the angular distribution of the radiation which leads to a change in the radiation pattern.[22,23] For the schematic case depicted in Fig. 3, the intensity of the radiation is given by

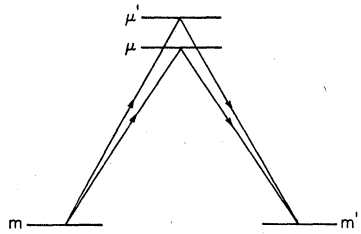

FIG. 3. Schematic representation of the excitation paths for the observation of the crossing of levels μ and μ'.

$$I(E_\mu - E_{\mu'}) = \text{const}\left(\frac{(\mathrm{Re}A)\Gamma^2}{(E_\mu - E_{\mu'})^2+\Gamma^2} + \frac{(\mathrm{Im}A)(E_\mu - E_{\mu'})\Gamma}{(E_\mu - E_{\mu'})^2+\Gamma^2}\right), \tag{13}$$

where E_μ is the energy divided by $\hbar$, Γ is the width of the excited state, and A is given by

$$A = \langle m'|\vec{\epsilon}_2\cdot\vec{r}|\mu'\rangle^*\langle m'|\vec{\epsilon}_2\cdot\vec{r}|\mu\rangle \times\langle\mu'|\vec{\epsilon}_1\cdot\vec{r}|m\rangle^*\langle\mu|\vec{\epsilon}_1\cdot\vec{r}|m\rangle\,. \tag{14}$$

Here $\vec{\epsilon}_1$ and $\vec{\epsilon}_2$ are, respectively, the polarization vectors for the absorbed and emitted photons. The phase of A depends upon the relative directions and polarizations of the emitted and absorbed photons. For A real, the level crossing signal is a Lorentzian curve; for A purely imaginary, the level crossing signal is a dispersion curve.

For the measurements reported here the incident and emitted photons were mutually orthogonal to one another and to the magnetic field. With this arrangement unpolarized incident and emitted light gives A real for the $|00\rangle|22\rangle$ crossing. The $|00\rangle|11\rangle$ crossing required polarized light. For this crossing we used linear polarizers with an angle of 45° with respect to the magnetic field to obtain a nonzero imaginary A. If large solid angles are used for the incident and scattered photons the signal is usually a mixture of Lorentzian and dispersion components.

IV. APPARATUS AND DATA-TAKING PROCEDURE

Figure 4 shows a schematic diagram of the apparatus. The sample volume was formed by a glass finger inserted into the magnetic field. A Varian vac-ion pump was used to evacuate the system prior to sealing it off and leaking in spectroscopically pure (<100 ppm impurities) ^{4}He to a prescribed pressure around 40 mtorr. The lowest pressure reached in the sample region was 2×10^{-8}

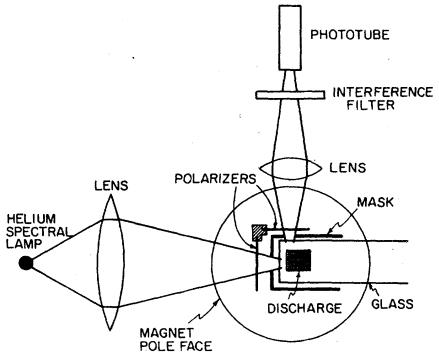

FIG. 4. Schematic diagram of the apparatus used to excite the helium atoms and to observe the level crossings in the $3\,^3P$ state.

torr. It is suspected that much of the residual pressure is due to outgassing of ^{4}He, which would not contaminate the sample. The measured rate of increase of pressure in the system when evacuated and sealed off was 0.2×10^{-6} torr/min. This was sufficiently low that over the period of a run there was no significant decrease in the metastable lifetime due to collisions with impurities.

A weak rf discharge was used in the sample region to excite He atoms to the $2\,^3S_1$ metastable state. The rf electrodes were mounted outside the glass tube and a 50-MHz radio-frequency field of roughly 100 V/cm was used to drive the discharge in the sample region. It is estimated that the electron density was approximately $10^7/\text{cm}^3$ and that $2\,^3S_1$ atoms were created at the rate of approximately $10^{12}/\text{cm}^3$ sec. It is further estimated that the lifetime of the metastable atoms in the sample volume was 2×10^{-4} sec,[24] and thus the average density was 2×10^8 metastable atoms/cm^3.

The magnetic field was provided by a Varian model V-4007-1 magnet with a gap of 7.6 cm and a pole face diameter of 15 cm. The magnet current was supplied by a well-regulated Varian V-2200A power supply. The net drift of the magnetic field was less than 5 ppm/h.

A 200-Hz magnetic field produced by a pair of coils wrapped around the pole caps was used to modulate the magnetic field. The coils were capacitively coupled to a driving audio amplifier to assure no dc contribution to the field. A Laboratory for Electronics model 101 marginal-oscillator nuclear-magnetic-resonance detector was employed with doped water and ^{7}Li samples to measure the magnetic field. The audio output of the detector was fed into a Princeton Applied Research model JB-4 phase-sensitive lock-in amplifier. During field measurement the output of the lock-in amplifier was used in conjunction with a varactor in parallel with the tank circuit of the marginal oscillator to lock the frequency of the marginal oscillator to the magnetic field. The NMR frequency was routinely measured to 0.5 ppm.

The probe, the sample tube, the stainless-steel vacuum system, and the gas-handling system were mounted on a moveable platform whose base was rigidly attached to the floor. The platform could be positioned so as to place either the sample or the NMR probe in the most homogeneous part of the magnetic field. The field calibration was carried out with the NMR probe in the position normally occupied by the sample.

A helium spectral lamp, driven by an rf discharge, was used as the source of 388.9-nm photons ($3\,^3P \rightarrow 2\,^3S$). The lamp was constructed from a glass container which was processed by pumping down to 10^{-8} torr and outgassing with a flame. The outgassing was repeated several times and spectroscopically pure helium was admitted to a pressure of 2 torr. A rf discharge was run for a few hours and then the system was pumped down with the rf excitation remaining on. The fill-discharge pump cycle was repeated until a bright rose-colored glow was evident on the walls after pump-down. Spectroscopically pure ^{4}He was then admitted to a pressure of 1.7 torr and the lamp was quickly removed from the vacuum system.

A 70-MHz oscillator was used to excite the lamp. The lamp gave sharp spectral lines with little background. These lamps lasted for approximately 100 h of operation and then showed signs of aging.

To increase the signal, the light from the brightest part of the spectral lamp was collected by a large glass lens and imaged onto the front face of the sample region. The incident solid angle was 120 msr. The sample region was delineated with black masks and the scattered light was collected by a second lens which subtended a solid angle of

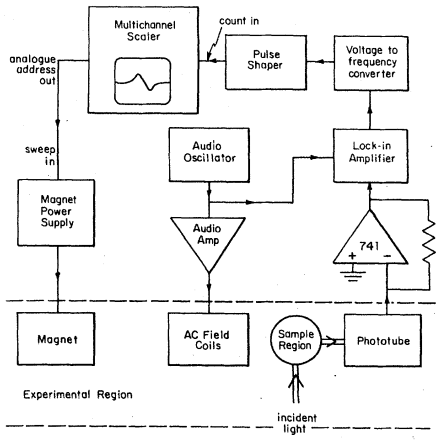

FIG. 5. Schematic diagram of the system used to record the data.

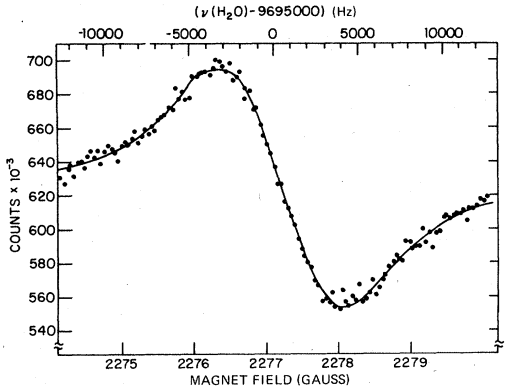

FIG. 6. Plot of the data for a typical run for the $|00\rangle|22\rangle$ crossing. The solid line is the parametrized fit to the data.

720 msr. The large extent of the solid angle made it necessary to perform an integration to determine the shape of the signal. For the $|00\rangle|22\rangle$ crossing the signal was Lorentzian when the average axes of the incident light, scattered light, and magnetic field were mutually orthogonal.

The scattered light passed through an interference filter selective to light with a wavelength of 388.9 nm and was detected by an RCA 6199 phototube with an S-11 response. Mu metal was used to shield the phototube from the stray magnetic field. Since the diffusion of the metastable atoms was small it was necessary for the discharge which created the metastable atoms to be in the center of the scattering region. As a result the dominant source of noise was due to fluctuations in the background light created by the discharge. For observation of the $|00\rangle|11\rangle$ crossing. Polaroid HNP polarizers were placed in front of both faces of the sample such that the transmission axis made an angle of 45° with the direction of the magnetic field.

Figure 5 shows a schematic diagram of the system used to take and record the data. The multichannel scaler controlled the cycle and swept the magnetic field. After a single sweep the multichannel scaler issued a done signal, waited a preset time, and then initiated another sweep. The delay was sufficient for the magnet power supply to restore the field to the value appropriate for the first channel. The cycle was repeated for roughly 15 sweeps (about $\frac{1}{2}$ h) during each run. The magnetic field corresponding to the center channel was measured before and after each run. Figure 6 shows the data for a typical run.

V. ANALYSIS OF THE DATA

A total of 93 runs was made; 89 were taken at the $|00\rangle|22\rangle$ crossing and 4 were taken at the $|00\rangle|11\rangle$ crossing. The $|00\rangle|11\rangle$ measurements were all taken at one pressure. The $|00\rangle|22\rangle$ measurements were distributed over eleven different pressures.

A multiparameter nonlinear least-squares fitting routine was used to analyze the data. The parameters entering the description of the line were the line center, the amplitude of the Lorentzian component, the amplitude of the dispersive component, and the background term. The signal can be expressed in the form

$$S(x)=\alpha/(1+x^2)+\beta x/(1+x^2)+\gamma_0+\gamma_1 x+\gamma_2 x^2\,, \tag{15a}$$

where

$$x=(H-H_0)/\Delta H\,. \tag{15b}$$

Here ΔH is the linewidth in gauss, H is the magnetic field in gauss, H_0 is the line center in gauss, α and β are constants which depend upon the geometry, and $\gamma_0, \gamma_1, \gamma_2$ describe the background. To determine the form of the recorded signal one must also take into account the modulation of the signal, the response time of the lock-in detector, and the time constant of the magnet. If the modulated magnetic field is described by the equation

$$x'=x+m\cos\omega t\,, \tag{16}$$

then following Arndt[25] it can be shown that the output of the lock-in detector at the fundamental frequency is given by

$$\frac{-(x+i)(\alpha-i\beta)}{m[m^2+(1-ix)^2]^{1/2}}+\text{c.c.}+\frac{2\beta}{m}+\gamma_1 m+2xm\gamma_2\,. \tag{17}$$

The time constant of the lock-in detector and the response of the magnetic field to a change in the sweep voltage result in a change in the line shape and a shift in the line center. The change in the line shape was incorporated in the theoretical line shape; the shift was added subsequent to the computer analysis of the data. Table II summarizes the parameters describing the line and their status in the fitting program. The background parameter γ_2 was set equal to 0 for the analysis of the data

TABLE II. Summary of the parameters used in describing the line.

Name	Symbol	Status
Signal intensity	$\alpha+\beta$	Free
Dispersion component	$\beta/(\alpha+\beta)$	Free
Line center	H_0	Free
Linewidth (HWHM)	ΔH	Free
dc offset	γ_1	Free
Modulation amplitude	m	Fixed
Background slope	γ_2	See text

TABLE III. Line centers for the individual data sets for the $|00\rangle|22\rangle$ crossing. The centers are given in terms of $\nu(H_2O)$-9695000 Hz. The different cardinal numbers refer to the different evacuations and refillings with helium.

Data set	Line center	Data set	Line center
1A	−15±162	6G	201±80
1B	61±234	6H	139±74
1C	169±208	7A	-112±162
1D	−49±178	7B	100±92
2A	291±270	7C	−2±92
2B	−111±414	8A	75±112
2C	171±384	8B	−57±130
3A	53±172	8C	27±116
3B	373±160	8D	317±126
3C	−71±90	8E	227±140
3D	187±172	9A	57±162
3E	57±76	9B	103±126
3F	−139±126	9C	435±176
3G	107±94	9D	145±162
3H	−79±106	9E	175±160
3I	29±132	9F	507±194
3J	109±86	9G	215±242
3K	13±86	10A	19±86
3L	105±102	10B	327±120
4A	205±140	10C	131±78
4B	85±112	10D	111±96
4C	111±136	11A	191±100
4D	121±130	11B	−119±94
4E	109±138	11C	29±102
4F	143±146	11D	139±90
4G	1±130	11E	21±62
4H	223±136	11F	−21±80
5A	95±120	11G	57±160
5B	65±122	12A	−151±98
5C	95±104	12B	37±78
5D	5±106	12C	21±92
5E	−19±126	12D	77±66
5F	121±92	13A	−23±108
5G	−87±98	13B	168±86
5H	41±106	13C	−19±105
5I	169±98	13D	160±71
5J	33±98	14A	148±134
5K	217±186	14B	87±80
5L	1113±810	14C	130±84
6A	19±76	14D	130±54
6B	79±92	14E	8±56
6C	125±94	14F	59±56
6D	111±80	14G	59±62
6E	237±76	14H	−77±130
6F	225±74		

for the $|00\rangle|22\rangle$ crossing; it was allowed to vary for the $|00\rangle|11\rangle$ crossing so as to take into account the increased field dependence due to distant plasma resonances.

Table III summarizes the observed line centers for the $|00\rangle|22\rangle$ crossing; Table IV summarizes the observed line centers for the $|00\rangle|11\rangle$ crossing. Figure 7 shows a histogram of the measurements

TABLE IV. Line centers for the $|00\rangle|11\rangle$ crossing. The centers are given in terms of $\nu(^7\text{Li})$-6 123 300Hz.

Data set	Line center
15A	−67±231
15B	132±141
15C	197± 91
15D	143± 99

of the $|00\rangle|22\rangle$ crossing.

Table V summarizes the pressures, average line centers, and linewidths for each of the series of measurements in which the sample was repositioned after evacuation and refilling with helium. It is estimated that the sample could be repositioned so that the average magnetic field was the same to ±2 ppm. An additional error has been added in quadrature to take into account this additional uncertainty.

Figure 8 shows a plot of the measured line centers versus pressure. There is no evidence for a dependence of the level crossing upon pressure. The average value for the level crossing obtained with the assumption of no pressure shift is

$$\nu_{H_2O} = 9\,695\,081 \pm 12 \text{ Hz} \quad (1.2 \text{ ppm}), \tag{18}$$

where the error is the one-standard-deviation statistical error. The average value for the level crossing obtained with the assumption of a linear

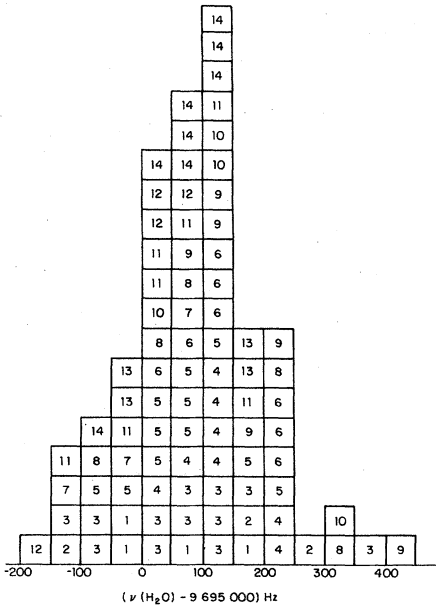

FIG. 7. Histogram for the corrected line centers for the $|00\rangle|22\rangle$ crossing. The numbers refer to the several repositionings of the apparatus subsequent to evacuation and refilling with helium.

TABLE V. Results of the computer fits for the $|00\rangle|22\rangle$ crossing for each of the independent evacuations and refillings with helium. The line center is expressed in terms of the proton resonance in water at the central magnetic field. The frequency has not been corrected for the diamagnetic shift due to the cylindrical sample.

Data set	Pressure (torr)	Dispersion component	Line width HWHM (G)	Line center (Hz)
1	0.0428(9)	0.0155(273)	1.161(27)	9 695 026 (97)
2	0.1020(25)	−0.0422(493)	2.149(38)	9 695 171 (196)
3	0.0458(6)	0.0784(77)	1.165(22)	9 695 044 (36)
4	0.0458(6)	0.0565(123)	1.158(23)	9 695 120 (51)
5	0.0458(3)	0.0774(63)	1.210(22)	9 695 061 (39)
6	0.0439(6)	0.0601(71)	1.127(22)	9 695 146 (34)
7	0.0417(19)	0.0647(157)	1.133(24)	9 695 027 (63)
8	0.0417(19)	0.0590(153)	1.138(23)	9 695 111 (59)
9	0.1104(16)	0.0323(133)	2.256(23)	9 695 206 (66)
10	0.0451(3)	0.0464(124)	1.176(23)	9 695 123 (50)
11	0.0815(6)	0.0376(70)	1.759(22)	9 695 034 (39)
12	0.0927(9)	0.0384(83)	1.868(23)	9 695 017 (45)
13	0.1260(16)	0.0314(58)	2.432(23)	9 695 098 (53)
14	0.0368(11)	0.0118(70)	1.037(22)	9 695 071 (32)

dependence on pressure is

$$\nu_{H_2O} = 9\,695\,084 \pm 30 \text{ Hz}. \tag{19}$$

Figure 9 shows a plot of the measured linewidth versus pressure. A least-squares fit gives for the half width at half maximum at zero pressure

$$\Delta H = 0.461 \pm 0.023 \text{ G}, \tag{20}$$

and for the slope

$$\frac{d(\Delta H)}{dp} = 15.7 \pm 1.7 \text{ G/torr}. \tag{21}$$

An additional uncertainty of, respectively, 0.01 G and 1.6 G/torr, has been included to account for the uncertainties in the modulation amplitude and in the calibration of the pressure gauge. The linewidth at zero pressure is determined by the lifetime of the $3\,^3P$ state. From the measured zero-pressure intercept we obtained

$$\tau(3\,^3P) = 97.6 \pm 4.5 \text{ nsec}. \tag{22}$$

This is in good agreement with the theoretical value[26]

$$\tau(3\,^3P) = 94.72 \text{ nsec}. \tag{23}$$

The dependence of the linewidth on the pressure gives a measure of the cross section for disruptive collisions which interrupt the radiation. With the assumption that the $^4He(3\,^3P)$-$^4He(1\,^1S_0)$ collisions are characterized by a kinetic gas temperature of 323 °K, the cross section for disorientation is $(718 \pm 78)\pi a_0^2$. This is a surprisingly large cross section.

The corresponding average for the $|00\rangle|11\rangle$ crossing was determined by a similar procedure. Table VI summarizes the results. With the assumption of no dependence on pressure, in terms of the resonance frequency for the ^7Li

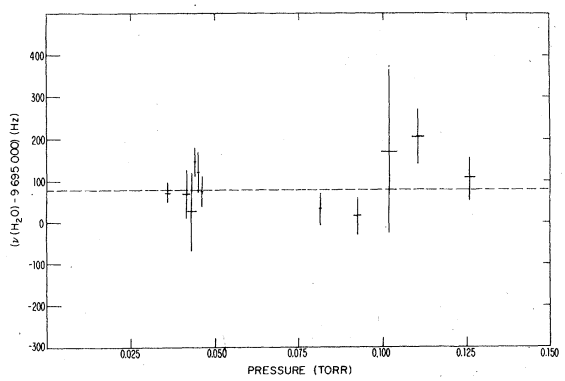

FIG. 8. Plot of the measured line centers vs helium pressure for the $|00\rangle|22\rangle$ crossing.

TABLE VI. Results of the computer fit for the $|00\rangle|11\rangle$ crossing. The line center is expressed in terms of the ^7Li resonance frequency at the central magnetic field. The frequency has not been corrected for the diamagnetic shift due to the cylindrical sample.

Pressure (torr)	Dispersion component	Linewidth HWHM (G)	Line center (Hz)
0.0550(22)	0.7833(171)	2.537(50)	6 123 428(71)

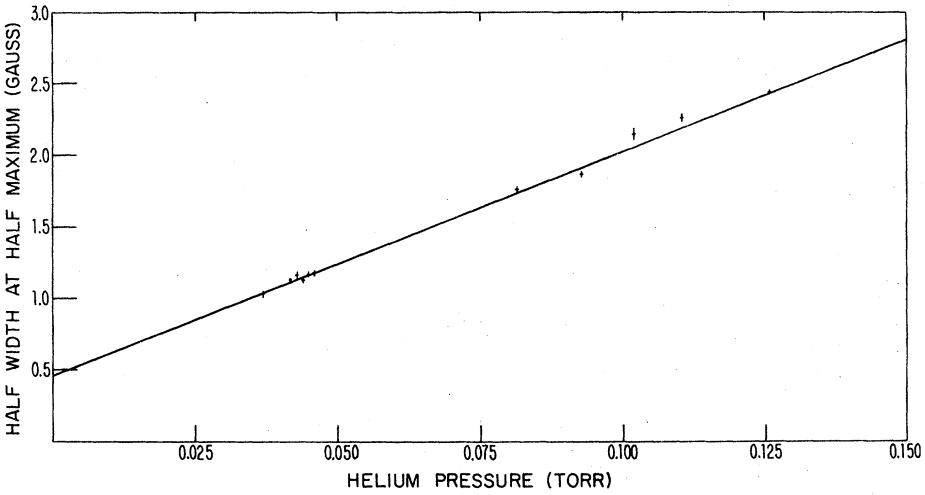

FIG. 9. Plot of the measured linewidth vs helium pressure for the $|00\rangle|22\rangle$ crossing. The straight line is a least-squares fit to the data.

probe the crossing is given by

$$\nu_{^7\mathrm{Li}} = 6\,123\,428 \pm 71 \text{ Hz} \quad (12 \text{ ppm}), \tag{24}$$

where the error is the one-standard-deviation statistical error.

VI. SYSTEMATIC UNCERTAINTIES

In this section we shall summarize the several sources of systematic uncertainties which limit the precision of the measurements.

A. Two-component line shape

Due to the finite solid angle subtended by the incident and scattered light beams, the level crossing signal is in general a superposition of a Lorentzian and a dispersion component. There is, unfortunately, a strong correlation between this admixture and the line center. From a computer simulation in which a modulated Lorentzian shifted from the correct center by 1% of the linewidth was fit with and without a dispersion component, we concluded that allowing the dispersion component to vary decreases the reliability with which the line center can be determined by a factor of 3. It should be noted that for the analysis of the data, we used both a Lorentzian and a dispersion component, so there is no correction due to the mixed line shape. The dominant effect of the uncertainty in line shape is to increase the uncertainty in the result.

B. Magnetic field

A careful study was made of the variation of the magnetic field over the sample volume. For the $|00\rangle|22\rangle$ crossing the magnetic field varied by less than 10 ppm over the 12 mm × 9 mm × 4 mm sample volume. A movement of the sample through 2 mm in either of the three orthogonal directions resulted in a 2.6-ppm change in the value for the average magnetic field.

The movement of the apparatus between data taking and field measurement was studied experimentally and found to change the average magnetic field by less than 0.4 ppm. Paramagnetic effects due to the apparatus, which might shield the sample region, were studied and shown to be less than 0.3 ppm. The magnetic field was cycled in the same manner during data taking and field measurement.

C. Time delay

The time constants of the lock-in amplifier and the magnet power supply introduced a time delay which shifted the line center. The measured time constant for the magnet was 0.173 ± 0.016 sec; for the lock-in amplifier 0.116 ± 0.010 sec. The combined delay results in a shift of 0.015 G (7 ppm) for the $|00\rangle|22\rangle$ crossing and 0.041 G (11 ppm) for the $|00\rangle|11\rangle$ crossing. The uncertainty in this correction is estimated to be 0.4 ppm for the $|00\rangle|22\rangle$ crossing and 0.7 ppm for the $|00\rangle|11\rangle$ crossing.

D. Field dependence of the apparatus

The phototube gain, discharge, and lamp intensity showed a weak dependence on magnetic field. Since the Q of the level crossing resonance was high, the magnetic field varied by only 0.3% during a sweep over the resonance. This reduced the importance of the variation with magnetic field. In addition the data-processing system was insensitive to signals linear in the magnetic field. It is estimated that the resulting additional uncertainty in the line center for the $|00\rangle|22\rangle$ crossing is

TABLE VII. Summary of the estimated systematic errors in parts per million for each of the two level crossings.

Source of uncertainty	Crossing $\|00\rangle\|22\rangle$	Crossing $\|00\rangle\|11\rangle$
Position dependence of magnetic field	2.6	10.0
Measurement of magnetic field	0.6	0.6
Data-recording system	1.1	1.8
Time delays	0.4	0.7
Field dependence of background	0.02	6.8
Nonlinearities	0.52	0.69
Harmonic sensitivity of lock-in amplifier	0.17	0.22
Long-term drift	0.39	1.2
Stark shifts	1.0	1.0
Zeeman curvature	0.04	0.16
Amplitude of modulation field	0.08	5.1
Quadratic sum	3.2	13.4

roughly 0.02 ppm. For the $|00\rangle|11\rangle$ crossing there is a larger background, and a term quadratic in the magnetic field has been included in the signal. It is estimated that the additional uncertainty in the line center is 6.8 ppm.

E. Sample environment

There are present in the sample volume, in addition to the metastable atoms being studied, ground-state atoms, free electrons, and atoms in various excited states. Collisions could result in a perturbation of the 3^3P state and a shift in the level crossing. This would give rise to a pressure shift or a dependence of the crossing point on the intensity of the discharge. Measurements taken as a function of pressure and discharge intensity indicated that such corrections were less than 1 ppm.

Table VII summarizes the several sources of systematic errors for the two crossings. Adding these uncertainties quadratically with the statistical uncertainty gives for the $|00\rangle|22\rangle$ crossing

$$\nu_{H_2O} = 9\,695\,081 \pm 33 \text{ Hz} \quad (3.4 \text{ ppm}), \tag{25}$$

and for the $|00\rangle|11\rangle$ crossing

$$\nu_{^7Li} = 6\,123\,428 \pm 109 \text{ Hz} \quad (18 \text{ ppm}). \tag{26}$$

VII. RESULTS FOR LEVEL CROSSING

To obtain the value of the magnetic field at the crossing point, one must first correct for the diamagnetic shielding in the sample volume. For the cylindrical samples used in this measurement the correction factor for the diamagnetic shielding is[27]

$$\nu_{corr} = \nu_{meas}(1 - 0.9 \times 10^{-6}). \tag{27}$$

With this correction, the resonance frequencies at the two level crossings become

$$\nu_{H_2O}(|00\rangle|22\rangle) = 9\,695\,072 \pm 33 \text{ Hz} \quad (3.4 \text{ ppm}), \tag{28}$$

$$\nu_{^7Li}(|00\rangle|11\rangle) = 6\,123\,422 \pm 109 \text{ Hz} \quad (18 \text{ ppm}). \tag{29}$$

The measured gyromagnetic ratios for the proton in water and ^{7}Li in water can then be used to determine the crossing field. Using[28,29]

$$\gamma'_{p,H_2O} = 2.675\,131\,4(11) \times 10^4 \text{ sec}^{-1}/\text{G} \tag{30}$$

and

$$\gamma'_{^7Li} = 1.039\,652\,6(11) \times 10^4 \text{ sec}^{-1}/\text{G}, \tag{31}$$

respectively, we obtain for the $|00\rangle|22\rangle$ crossing

$$H(|00\rangle|22\rangle) = 2277.1193(78) \text{ G} \quad (3.4 \text{ ppm}), \tag{32}$$

and for the $|00\rangle|11\rangle$ crossing

$$H(|00\rangle|11\rangle) = 3700.7168(660) \text{ G} \quad (18 \text{ ppm}). \tag{33}$$

For the determination of the zero-field fine-structure intervals, one needs not H but $\mu_B H/h$. For this calculation the somewhat more precisely known proton and ^{7}Li g factors can be used. In particular,[30]

$$g_{p,H_2O} = 3.041\,986\,44(20) \times 10^{-3} \quad (0.1 \text{ ppm}), \tag{34}$$

$$g_{^7Li} = 1.182\,225\,75(122) \times 10^{-3} \quad (1 \text{ ppm}). \tag{35}$$

These values are used later in the determination of the zero-field fine-structure splittings.

The result for the $|00\rangle|22\rangle$ crossing can be compared with other measurements. Kaul[31] used a fast H_2^+ beam to coherently excite the $|00\rangle|22\rangle$ states directly from the ground state and obtained

$$H(|00\rangle|22\rangle) = 2277.0300(700) \text{ G}. \tag{36}$$

Lhuiller *et al.*[32,33] used a proton beam to directly excite the atoms to these two states and obtained

$$H(|00\rangle|22\rangle) = 2277.1250(150) \text{ G}. \tag{37}$$

The agreement between the three measurements is satisfactory.

VIII. DETERMINATION OF THE FINE-STRUCTURE INTERVAL

The magnetic field at which the two Zeeman levels cross can be expressed in the form

TABLE VIII. A summary of the measurements of the fine structure in the ^3P state of ^{4}He. All the intervals are expressed in MHz.

Interval	Value	Reference
$^3P_1$–$^3P_2$	658.0 ±5.0	35
	658.55±0.15	34
	658.63±0.27	This experiment
$^3P_0$–$^3P_1$	8100.0 ±16.0	36
	8113.78±0.22	34
	8113.75±0.31	31
	8113.92±0.29	This experiment
$^3P_0$–$^3P_2$	8772.33±0.37	34
	8772.56±0.06	33
	8772.552±0.040	This experiment
	8772.560±0.037	This experiment

$$H_i = Z_i(g'_L, g'_S, g_x, R_{14}, R_{15}, E_{02}, E_{12}), \quad (38)$$

where R_{14} and R_{15} are radial integrals associated with the quadratic term in the Hamiltonian, E_{02} and E_{12} are the zero-field fine-structure intervals, and the index i identifies the crossing. Using the results of this experiment and parameters listed in Table I, we obtained

$$E_{02} = 8772.552(40) \text{ MHz} \quad (4.5 \text{ ppm}), \quad (39a)$$

$$E_{12} = 658.634(271) \text{ MHz} \quad (412 \text{ ppm}), \quad (39b)$$

$$E_{01} = 8113.917(291) \text{ MHz} \quad (36 \text{ ppm}). \quad (39c)$$

The quoted errors are one standard deviation and include the estimated systematic uncertainties.

By observing rf transitions at low magnetic field, Wieder and Lamb[34] obtained for the fine-structure intervals in the $3\,^3P$ state

$$E_{02} = 8772.330(370) \text{ MHz} \quad (42 \text{ ppm}), \quad (40a)$$

$$E_{12} = 658.550(150) \text{ MHz} \quad (228 \text{ ppm}), \quad (40b)$$

$$E_{01} = 8113.780(220) \text{ MHz} \quad (27 \text{ ppm}). \quad (40c)$$

From a level crossing measurement, Kaul[31] obtained for the $^3P_0$-$^3P_1$ interval

$$E_{01} = 8113.75(31) \text{ MHz} \quad (38 \text{ ppm}). \quad (41)$$

Lhuillier *et al.*[33] obtained from their level-crossing experiment

$$E_{02} = 8772.56(6) \text{ MHz} \quad (6.8 \text{ ppm}). \quad (42)$$

Berry *et al.*[35] and Wittman *et al.*[36] used the beam-foil technique to measure, respectively, the $^3P_1$-$^3P_2$ and the $^3P_0$-$^3P_1$ intervals. They obtained

$$E_{12} = 658.0(50) \text{ MHz} \quad (7600 \text{ ppm}), \quad (43)$$

$$E_{01} = 8100(16) \text{ MHz} \quad (1980 \text{ ppm}). \quad (44)$$

The agreement between the several measurements is satisfactory.

The value for E_{12} obtained by Wieder and Lamb[34] can be used in conjunction with the $|00\rangle|22\rangle$ crossing determined in this experiment to obtain a more precise value for E_{02}. This analysis gives

$$E_{02} = 8772.560(37) \text{ MHz} \quad (4.2 \text{ ppm}), \quad (45)$$

where the quoted uncertainty is one standard deviation. Table VIII summarizes the several determinations of the fine structure in the $3\,^3P$ state of He.

The theoretical calculations for these fine-structure intervals are less precise than the experimental values. Accad *et al.*[6,21] obtained

$$E_{02} = 8772.65(30) \text{ MHz} \quad (34 \text{ ppm}), \quad (46a)$$

$$E_{12} = 658.14(30) \text{ MHz} \quad (456 \text{ ppm}), \quad (46b)$$

$$E_{01} = 8114.51(30) \text{ MHz} \quad (37 \text{ ppm}). \quad (46c)$$

This calculation does not include the α^6 terms which could potentially contribute 2.6 MHz. The quoted uncertainty in the theoretical results stems from the failure of the Ritz variational method when applied to excited states without unique symmetry. The convergence of the Hylleraas wave functions in $3\,^3P$ states is affected by the presence of the $2\,^3P$ state with the same symmetry and lower energy. The agreement between theory and experiment is adequate but the theoretical calculations are not sufficiently precise to provide an interesting test of the theory.

IX. CONCLUSIONS

We have reported a new determination of the fine structure in the $3\,^3P$ state of helium which is in agreement with, but more precise than, earlier measurements. At present the measurements are more precise than the theoretical calculations for these fine-structure intervals; thus the measurements cannot be used to make a significant test of the theory.

If the theoretical prediction for the fine-structure interval in the $n = 3$ state of helium could be improved so that it is more precise than this experiment, these measurements could be used to determine the fine-structure constant to 2 ppm. The fine-structure interval in the $n = 2$ state of helium has been measured to a precision[15,16] of 1 ppm and in conjunction with the theoretical calculations yields a value of α with a precision of 0.94 ppm.[10] The results for the $n = 3$ interval would constitute an independent test of the theory of the two-electron atom used in the determination of α.

ACKNOWLEDGMENT

This research was supported in part by the National Science Foundation under Grant No. MPS74-13728.

*Present address: Dept. of Physics, MIT, Cambridge, Mass. 02139.

[1]H. A. Bethe and E. E. Salpeter, *Quantum Mechanics of One- and Two-Electron Atoms* (Springer, Berlin, 1957).
[2]N. M. Kroll, in *Atomic Physics*, edited by S. J. Smith and G. K. Walters (Plenum, New York, 1973), Vol. 3, p. 33.
[3]V. W. Hughes, in *Atomic Physics*, edited by S. J. Smith and G. K. Walters (Plenum, New York, 1973), Vol. 3, p. 1.
[4]M. L. Lewis, *in Atomic Physics*, edited by G. zu Putlitz, E. W. Weber, and A. Winnacker (Plenum, New York, 1975), Vol. 4, p. 105.
[5]C. Schwartz, Phys. Rev. 134, A1181 (1964).
[6]B. Schiff, C. L. Pekeris, and H. Lifson, Phys. Rev. 137, A1672 (1965).
[7]L. Hambro, Phys. Rev. A 5, 2027 (1972).
[8]L. Hambro, Phys. Rev. A 6, 865 (1972).
[9]L. Hambro, Phys. Rev. A 7, 479 (1973).
[10]M. L. Lewis, P. H. Serafino, and V. W. Hughes, Phys. Lett. 58A, 125 (1976).
[11]J. Daley, M. Douglas, L. Hambro, and N. M. Kroll, Phys. Rev. Lett. 29, 12 (1972).
[12]M. Douglas and N. M. Kroll, Ann. Phys. (N.Y.) 82, 89 (1974).
[13]M. Douglas, Phys. Rev. A 6, 1929 (1972).
[14]A. Dalgarno and J. T. Lewis, Proc. R. Soc. Lond. A 233, 70 (1956).
[15]F. M. J. Pichanick, R. D. Swift, C. E. Johnson, and V. W. Hughes, Phys. Rev. 169, 55 (1968).
[16]A. Kponou, V. W. Hughes, C. E. Johnson, S. A. Lewis, and F. M. J. Pichanick, Phys. Rev. Lett. 26, 1613 (1971).
[17]S. A. Lewis, F. M. J. Pichanick, and V. W. Hughes, Phys. Rev. A 2, 86 (1970).
[18]M. L. Lewis and V. W. Hughes, Phys. Rev. A 8, 2845 (1973).
[19]M. L. Lewis and V. W. Hughes, Phys. Rev. A 11, 383 (1975).
[20]R. S. Van Dyck, Jr., P. B. Schwinberg, and H. G. Dehmelt, Phys. Rev. Lett. 38, 310 (1977).
[21]Y. Accad, C. L. Pekeris, and B. Schiff, Phys. Rev. A 4, 516 (1971).
[22]M. E. Rose and R. L. Carovillano, Phys. Rev. 122, 1185 (1961).
[23]G. zu Putlitz, in *Atomic Physics*, edited by B. Bederson, V. W. Cohen, and F. M. J. Pichanick (Plenum, New York, 1969), Vol. 1, p. 227.
[24]A. V. Phelps and J. P. Molnar, Phys. Rev. 89, 1202 (1953).
[25]R. Arndt, J. Appl. Phys. 36, 2522 (1965).
[26]W. L. Wiese, M. W. Smith, and B. M. Glennon, *Atomic Transition Probabilities*, NSRDS-NBS4 (U.S. G.P.O., Washington, D.C., 1966).
[27]E. R. Andrew, *Nuclear Magnetic Resonance*, (Cambridge U. P., Cambridge, 1969), p. 78.
[28]P. T. Olsen and E. R. Williams, in *Atomic Masses and Fundamental Constants*, edited by J. H. Sandars and A. M. Wapstra (Plenum, New York, 1976), Vol. 5, p. 538.
[29]G. H. Fuller and V. W. Cohen, Nucl. Data A 5, 433 (1969).
[30]E. R. Cohen and B. N. Taylor, J. Phys. Chem. Ref. Data 2, 663 (1973).
[31]R. D. Kaul, J. Opt. Soc. 57, 1156 (1967).
[32]C. Lhuillier, P. Riviere, and J. P. Faroux, C. R. Acad. Sci. B276, 607 (1973).
[33]C. Lhuillier, J. P. Faroux, and N. Billy, J. Phys. (Paris) 37, 335 (1976).
[34]I. Wieder and W. E. Lamb, Jr., Phys. Rev. 107, 125 (1957).
[35]H. G. Berry, J. L. Subtil, and M. Carre, J. Phys. (Paris) 33, 947 (1972).
[36]W. Wittmann, K. Tillmann, H. J. Andrä, and P. Dobberstein, Z. Phys. 257, 279 (1972).